JOURNAL OF SPACECRAFT AND ROCKETS
Vol. 45, No. 1, January–February 2008

Qualification of Spacecraft Equipment: Random-Vibration Response Based on Impedance/Mobility Techniques

G. Rodrigues*
Free University of Brussels, 1050 Brussels, Belgium
and
J. Santiago-Prowald†
ESA, 2200 AG Noordwijk, The Netherlands

DOI: 10.2514/1.29734

Random vibrations are a driving-load case in the development of spacecraft equipment. The approaches currently used in preliminary design for deriving vibration levels range in complexity from the Miles formula to multi-degree-of-freedom models. Meanwhile, impedance/mobility techniques can facilitate the modeling of complex systems by characterizing each subsystem in a compact and modular way. The solution of the coupled response is then obtained by multiplication of impedance and mobility matrices, thus avoiding an eigenvalue extraction for the entire system. This paper describes a dynamic condensation technique for studying the coupled response of a carrier structure represented by its modal mobility and the equipment represented by its impedance at the interface. Only basic modal parameters are needed for each subsystem, enabling the application of this method in any phase of project life. In preliminary phases, simple formulas or heritage information can be used, whereas in advanced phases, they can be computed from finite element analysis or measured during tests. This method eases integration of subcontractors' data, enables quick sensitivity computations, and allows predicting acceleration and force levels for dynamic tests. A numerical example for the case of a satellite panel with multi-degree-of-freedom equipment is compared with detailed finite element analysis.

Nomenclature

A	=	integrating range of the carrier
$\mathbf{a}$	=	modal coordinates vector
F	=	force
$\mathbf{F}$	=	force vector at the interface points
f	=	frequency
$\mathbf{G}$	=	compliance matrix
g	=	acceleration of gravity
H	=	frequency response function
j	=	imaginary unit
$\mathbf{L}$	=	modal participation factor
$\tilde{\mathbf{M}}$	=	apparent mass
m	=	mass
$\mathbf{m}_B$	=	residual mass of higher-order modes
p	=	acoustic pressure
r	=	distance between two points on the panel
S	=	power spectral density
$U, \dot{U}, \ddot{U}$	=	displacement, velocity, and acceleration frequency response functions
$\mathbf{U}$	=	vectors of displacement, velocity, and acceleration frequency response functions at the interface points
$u, \dot{u}, \ddot{u}$	=	displacement, velocity, and acceleration
$\mathbf{Y}$	=	mobility matrix
$\tilde{\mathbf{Y}}$	=	modal mobility matrix
Y	=	driving-point mechanical mobility
y	=	coordinate in the panel
Z	=	driving-point mechanical impedance
$\mathbf{Z}$	=	impedance matrix of the instrument at the interface points
α	=	mass ratio between the load and carrier, m_2/m_1
Γ	=	generalized force
γ	=	surfacic mass density of the panel
ζ	=	hysteretic modal damping coefficient
λ	=	frequency ratio between the load and carrier, f_2/f_1
ξ	=	viscous modal damping coefficient
$\mathbf{\Phi}$	=	vector of mode shapes
ϕ	=	mode shape
Ω	=	frequency of excitation normalized with the natural frequency of the carrier
ω	=	angular frequency

Subscripts

c	=	coupling
e	=	equipment
ex	=	external force
f	=	flexural
k	=	index of equipment units
r	=	rigid body
0	=	base
1	=	carrier
2	=	instrument

I. Introduction

RANDOM vibrations taking place at launch are a driving-load case for spacecraft equipment, payloads, secondary structures, and interfaces. They are produced by the propulsion system and the vehicle aerodynamics, especially during liftoff and transonic flight. Nevertheless, experience shows that the first 10 s after liftoff is the most demanding phase for most launchers in regard to acoustic pressure levels. The rocket engine plumes and exhaust-duct jets radiate an intense acoustic field that impinges on the external surface of the launch vehicle, both directly reflected by the launch pad and ground. Measurements [1–3] have shown that this acoustic pressure load is random and broadband in nature, becoming reasonably steady and ergodic after the initial blast waves. In addition, oscillations

Received 21 January 2007; revision received 9 July 2007; accepted for publication 4 August 2007.

*Research Engineer, Active Structures Laboratory, Code Postale 165/42, 50 Avenue F. D. Roosevelt; Goncalo.Rodrigues@ulb.ac.be.

†Project Manager, Structures Section, European Space Research and Technology Center; Julian.Santiago.Prowald@esa.int. Member AIAA.

occurring in the combustion chamber generate vibrations that transmit through the structure of the launcher up to the spacecraft.

The acceleration levels experienced by a unit will be a result of the loads applied to its carrier structure (which is normally a spacecraft secondary structure) and of the way the carrier and the equipment units are coupled dynamically. In the cases in which the carrier consists of a lightweight panel, the direct response of the panel to the acoustic field inside the fairing becomes the dominant transmission path of random vibrations.

The random-vibration environment (RVE) of equipment is normally specified as a base acceleration. For simplicity, common approaches do not take the coupling with the supporting structures into account. The resulting uncertainty needs to be covered by large safety factors that lead to the overdesign and the overtest of the equipment with the inherent mass penalty.

Miles formula [4] is a simple analytical tool that provides the root-mean-square (rms) response of a hard-mounted single-degree-of-freedom system that is excited by random white-noise at the base. NASA [5] proposed an extension to a multi-degree-of-freedom representation of the instruments. By implementing a simple numerical procedure, the response can be obtained in terms of rms and in terms of power spectral density (PSD). This approach provides a more realistic distribution of the response across the frequency spectrum, although the different modal contributions of the system are superposed in a worst-case in-phase condition. In both the single and the multi-degree-of-freedom versions, neglecting the mechanical coupling between the carrier and the equipment reveals to be excessively overconservative. On the other hand, assuming that the system has the same levels of excitation across the whole frequency spectrum (white-noise assumption) might even yield underpredictions in some configurations [6].

The mechanical coupling between one mode of the instrument and one mode of the carrier has been studied by several authors [7–10]. Simple analytical formulas have been used for describing the dynamics of the two-degree-of-freedom system. These succeeded in identifying the dynamic absorber effect, but like the multi-degree-of-freedom extension of the Miles formula, the white-noise assumption made on the excitation is incompatible with the existence of a multimodal response. Also, the one-degree-of-freedom representation of each the carrier and the instrument confers mainly a qualitative interest to the results obtained with this method.

Ruotolo and Cotterchio [11,12] presented a numerical procedure for computing the coupled response of one multi-degree-of-freedom instrument mounted on a multi-degree-of-freedom carrier. Their method consists of the extraction of the eigenvalues of the coupled system based on the standalone modal properties of each subsystem. Although it provides a valuable tool for design and optimization, it is limited to configurations with a single multi-degree-of-freedom instrument or to several single-degree-of-freedom instruments.

The most accurate process for computing the coupled mechanical response is performing a finite element analysis (FEA) with a detailed model for the carrier or even the entire satellite. However, it is very time-consuming, both in the modeling and the calculation phases. This reduces the applicability to the low-frequency spectrum, and hence the instruments are commonly modeled by a single oscillator or even rigid masses.

The concepts of impedance and mobility allow a compact formulation for representing physical systems. They were first applied to the study of electrical systems and later to electromechanical or mechanical systems [13,14]. Kim and Brennan [15,16] employed this formulation for modeling and controlling the coupled response of structural-acoustic systems. This paper is a continuation of previous work done by the authors [17]. It contains a generalized formulation, covers a wider range of cases, and outlines the importance of a correction term in enhancing the results previously shown. An analytical condensation technique is presented for describing the dynamic coupling between carrier structures and equipment that is based on the impedance and mobility concepts. These techniques enable the modeling of one carrier with several normal modes and many instruments with several normal modes each, providing the force and the acceleration at the interfaces between the instruments and carrier, both in PSD and rms, and can be applied for any spectral distribution of the acceleration input. The coupled response is obtained simply by multiplying the impedance and the mobility matrices and inverting matrices that have a dimension on the order of the number of instruments. This avoids the computation of the eigenvalues for the complete subsystem. The modal information for each subsystem is condensed only once. This results in a modular approach suitable for complex projects, enabling the integration of information from different subsystems developed by different subcontractors, even at different levels of maturity. The modal condensation of each subsystem can range from simple analytical models or heritage information from older projects up to results from FEA or mechanical tests.

This paper starts with a qualitative investigation of the mechanical coupling still based on the two-degree-of-freedom system. The causes for overdesign and overtest of equipment are once more put in evidence. Additionally, we present a chart that allows a quick estimation of the natural frequencies of the coupled system and thus the establishment of guidelines for equipment design. Next follows the development of the method for simulating the mechanical coupling, which is based on impedance and mobility techniques. An impedance matrix is defined for the set of the instruments, and a modal mobility matrix is presented for the carrier. The static residual of the carrier at the interface points to the instruments is introduced for overcoming convergence and accuracy problems. Finally, after defining the generalized forces associated to the base acceleration and point forces, the frequency response functions of the response can be written and from them the random response can be evaluated. The results obtained with this method are finally compared with FEA of the same system for validation purposes and a convergence study is performed to judge the influence of the static residual term.

II. Two-Degree-of-Freedom System Revisited

The simplest model for analyzing the dynamic coupling between the carrier structure and the equipment unit consists of a two-degree-of-freedom system excited at the base. The base excitation of a normal mode of the carrier structure and the coupling with a normal mode of the equipment can be correctly simulated by placing the two oscillators of the two-degree-of-freedom system in series.

This simple system has been the object of study by many authors. Ceresetti [7] derived the random-vibration environment of equipment units in terms of rms based on the levels of the acceleration observed at the carrier interface. The study of the two-degree-of-freedom system provides the ratio between these two quantities Q_{eff}, taking into account the beneficial dynamic coupling between the instrument and the carrier. On the other hand, Chang [8] and Scharton [9] employed simple dynamic systems for estimating the force exerted by instruments excited at the base and used it as a reference in the closed-loop force-controlled vibration testing.

If the nomenclature of the theory of electric circuits is adopted in the study of the two-degree-of-freedom system, the instrument becomes commonly identified as the load and the carrier becomes identified as the carrier, as depicted in Fig. 1. The study presented herein will address both the frequency response and the rms response of the carrier and the load and their dependence on nondimensional mass, stiffness, and frequency parameters.

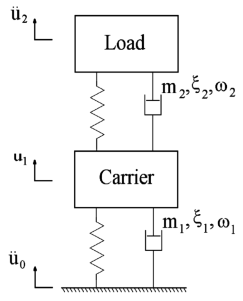

Fig. 1 Two-degree-of-freedom system with the two oscillators in series.

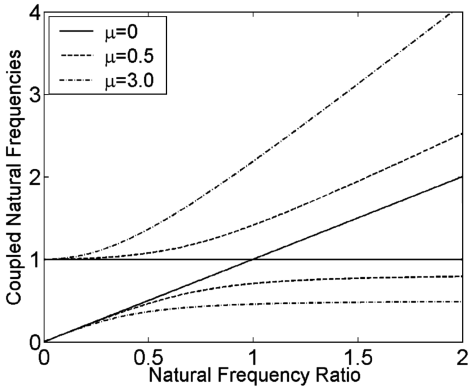

Fig. 2 Natural frequencies of the coupled system in terms of the nondimensional parameters.

A. Equations of Motion and Resonances of the Coupled System

The equations of motion can be written for the two masses in terms of the nondimensional parameters: 1) the ratio between the mass of the load and the mass of the carrier, $\alpha = m_2/m_1$; 2) the ratio between the natural frequencies of load and carrier, $\lambda = f_2/f_1$; 3) the frequency of excitation/response normalized by the natural frequency of the carrier, Ω; and 4) the viscous damping coefficients ξ_1 and ξ_2.

The equations of motion in terms of the nondimensional parameters thus become

$$\begin{bmatrix} -\Omega^2 & 0 \\ 0 & -\Omega^2 \end{bmatrix}\begin{bmatrix} U_1 \\ U_2 \end{bmatrix} + \begin{bmatrix} j2(\xi_1 + \mu\lambda\xi_2)\Omega & -j2\mu\lambda\xi_2\Omega \\ -j2\lambda\xi_2\Omega & j2\lambda\xi_2\Omega \end{bmatrix}\begin{bmatrix} U_1 \\ U_2 \end{bmatrix} + \begin{bmatrix} 1+\mu\lambda^2 & -\mu\lambda^2 \\ -\lambda^2 & \lambda^2 \end{bmatrix}\begin{bmatrix} U_1 \\ U_2 \end{bmatrix} = \begin{bmatrix} U_0(1+j2\xi_1\Omega) \\ 0 \end{bmatrix} \tag{1}$$

The use of the nondimensional parameters enables the presentation of the coupled system natural frequencies in a very compact form. These are graphed in Fig. 2 as a function of the frequency ratio. The two eigenvalue curves are presented for different values of mass ratio between load and carrier.

As can be observed, the two subsystems become more coupled as the mass of the load increases in comparison with the mass of the carrier. This fact is shown by the divergence of the solution curves from the straight-lines representing the null mass ratio.

Essentially, two limit cases can be identified in this chart. For λ much greater than one, the carrier behaves as if it had a larger mass (the rigid load) and its natural frequency decreases. This corresponds to the lower curves on the right side of the chart. The upper curves are the natural frequencies associated to the motion of load. For λ much lower than the unity, the interaction between the two masses becomes negligible and a decoupling of the system takes place. This situation corresponds to the left side of the chart.

The qualitative understanding of this graph is very useful in a preliminary design phase, because it allows for an immediate estimation of the resulting natural frequencies of the carrier-instrument system in terms of the modal properties of the standalone carrier and instrument.

B. Frequency Response Functions

The solution of Eq. (1) provides the frequency response function of the load and carrier centers of mass to a base acceleration transmitted by the primary structure at its interface to the carrier.

Figure 3 shows these nondimensional frequency response functions for a specific set of nondimensional parameters ($\alpha = 0.5$, $\lambda = 2.0$, and $\xi_1 = \xi_2 = 0.05$).

For a frequency of excitation equal to the uncoupled natural frequency of the load, the carrier shows an antiresonance. This is the so-called dynamic absorber effect and consists of low response of the carrier for frequencies around the natural frequency of the load alone. However, it is a common practice to envelope the accelerations levels at the interface between the instrument and the carrier in the frequency domain and to apply this envelope as specification for instrument qualification testing, without taking into account the coupling with the load. This results in overexciting the instrument at its natural frequency and thus it is a major cause of instrument overtesting as identified by several authors [7–10].

The study of the load alone can be described by Eq. (2), which shows that the response of the load depends only on its mechanical parameters and the acceleration levels applied to it at the interface to the carrier:

$$\frac{\ddot{U}_2(\omega)}{\ddot{U}_1(\omega)} = \frac{(\omega_2^2 + j2\xi_2\omega_2\omega)}{-\omega^2 + j2\xi_2\omega_2\omega + \omega_2^2} \tag{2}$$

However, real instruments mounted on real panels present a distributed fixation that cannot be adequately modeled by a two-degree-of-freedom system. Brevart and Pradines [18] identified that, in this case, the infinite impedance of the shaker is also a cause for overtesting. In the shaker test configuration, the accelerations are applied in-phase and the input levels result from enveloping the levels of different interface locations in the flight configuration.

C. RMS Response

Figures 4 and 5 show the rms of the response of the carrier and the load for different values of the nondimensional parameters. These rms values were analytically derived using the method described by Newland [19].

It can be observed in Fig. 4 that when the load has a natural frequency close to that of the carrier, the resonance of the carrier is damped due to the dynamic absorber effect, resulting in a lower response of the carrier. However, this coincidence of natural frequencies results in a higher response of the load. This means that for a prescribed acceleration of the carrier at the interface to the primary structure, the random-vibration environment of the

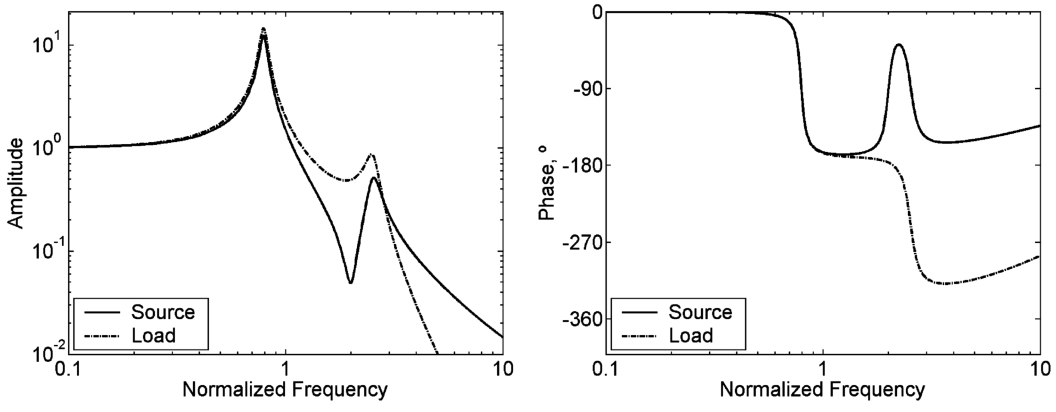

Fig. 3 Frequency response function for $\xi_1 = \xi_2 = 0.05$, $\lambda = 2.0$, and $\mu = 0.5$.

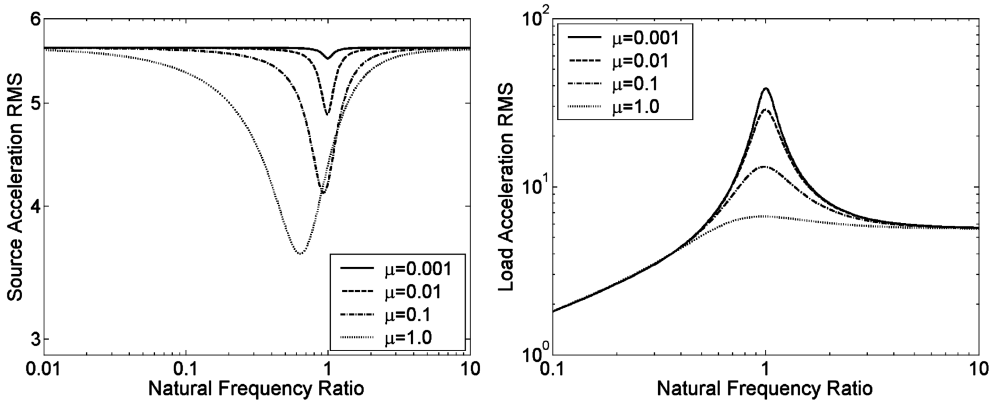

Fig. 4 Effect of the mass ratio on the carrier and load rms for $S_0 = 1$ and $\xi_1 = \xi_2 = 0.05$.

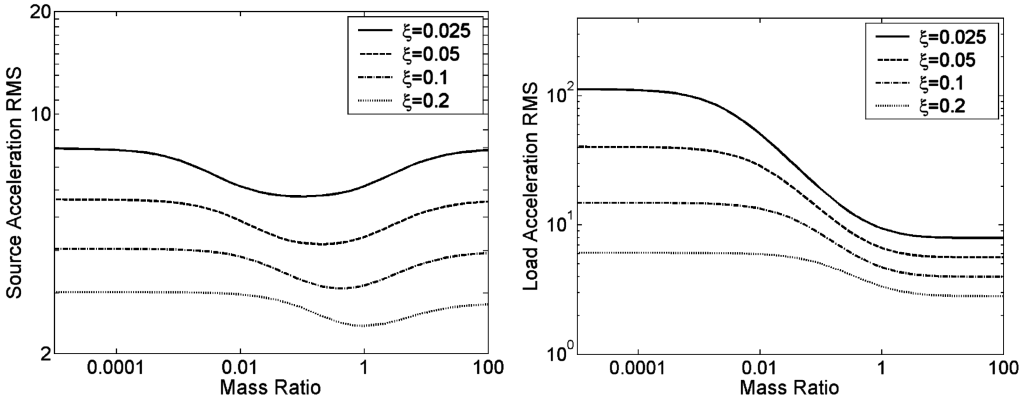

Fig. 5 Effect of the damping on the carrier and load rms for $S_0 = 1$ and $\lambda = 1$.

instrument will be maximum when its natural frequency coincides with that of the carrier, despite lower response of the carrier and thus lower levels applied to the instrument.

Figure 5 also shows that for a prescribed acceleration of the carrier at the interface to the primary structure, the response of the instrument will be lower when its mass increases. This fact is in accordance with the mass acceleration curve [20].

D. Conclusions and Limitations

The study of the lumped mass two-degree-of-freedom system provides great insight on the interaction between one normal mode of the carrier and one normal mode of the instrument. It highlights the main cause for instrument overtesting and provides a simple qualitative prediction tool for the dependence of the response on the parameters of the equipment and the carrier. However, the simplicity also reduces the scope of applicability of these tools. The fact that only one mode of the load and one mode of the carrier are being considered makes it impossible to correctly predict what happens when the instrument or the carrier obey more complicated dynamic descriptions.

The assumption of white noise taken in the computation of the rms is appropriate when the response of the system is concentrated in a narrow frequency band and thus only requires information on the input on that frequency band. This is the basis for the Miles equation. However, because the multi-degree-of-freedom system has several resonances that can be very different in frequency, the knowledge of the different inputs at those frequencies becomes important and makes a generalization for the complete frequency spectrum impossible. Finally, the knowledge of the location of the instrument on the carrier also has a crucial role as different points of the carrier show different response. A more complex but also more representative model is thus required to obtain accurate predictions.

III. Derivation of the Impedance/Mobility Method

Impedance and mobility analysis techniques allow analyzing the coupling between linear substructures by means of a simple and compact matrix manipulation. In this section, a method is derived for computing the response of a coupled system based on the information obtained for each subsystem separately. The starting point is the definition of driving-point impedance and mobility. These concepts are then extended to a coupling at the interfaces in the six degrees of freedom, and the transfer functions between the external forces and base acceleration to the carrier structure are derived by simple algebraic matrix manipulation. The random response follows directly from the transfer function definition. Only base acceleration and concentrated forces are considered. The case of distributed loads with spatial random distribution could be derived following the methods of Piersol and Bendat [21], as previously shown by the authors [17]. Also, the extension to multi-input/multi-output systems would follow the approach presented by Newland [19].

A. Coupled Equations of the System

Driving-point impedance and mobility of a system are defined as the ratios between the driving force and the velocity at the point of application of the force [13]:

$$Z = \frac{F}{\dot{U}}, \qquad Y = \frac{\dot{U}}{F} \tag{3}$$

In the case of a carrier with several instruments, the forces at each interface can be described in matrix form in terms of the velocity at those interface points and the impedance of the respective loads:

$$\mathbf{F}_1 = \mathbf{Z}_e \dot{\mathbf{U}}_1 \tag{4}$$

In the same way, the dynamic response of the carrier structure can be obtained by the multiplication of its mobility and the different applied forces:

$$\dot{\mathbf{U}}_1 = \mathbf{Y}_1 \mathbf{F} \tag{5}$$

Because the carrier is a structure with a distributed interface, the analysis can be greatly simplified if displacements and velocities are decomposed in terms of the mode shapes of the carrier. The response in velocity at the interfaces becomes a product of the mode shapes of the carrier and the first time derivative of the modal coordinates:

$$\dot{\mathbf{U}}_1 = \mathbf{\Phi}^T \dot{\mathbf{a}} \tag{6}$$

For the case of base excitation, the rigid-body modes have to be taken into account. Thus, $\mathbf{\Phi}$ is defined as a matrix that contains the rigid-body and the flexural mode shapes at the interface locations between the carrier and the instruments:

$$\mathbf{\Phi} = \begin{bmatrix} \mathbf{\Phi}_r \\ \mathbf{\Phi}_f \end{bmatrix} \tag{7}$$

They are normalized with the objective of producing unitary modal masses:

$$\int_A \phi_{1,n}^2(y)\gamma(y)\,\mathrm{d}y = 1 \tag{8}$$

The time derivative of the modal coordinates can be easily obtained in terms of the generalized applied forces if the dynamic properties of the carrier structure are described in terms of a modal mobility [16]:

$$\dot{\mathbf{a}} = \bar{\mathbf{Y}}_1 \Gamma \tag{9}$$

In the case of a spacecraft, three different sources of generalized forces can be considered to be applied to the carrier structure. The base excitation Γ_0 results from the vibrations of the primary structure of the spacecraft that are transmitted to the carrier structure. The external forces Γ_{ex} can be, for example, the acoustic excitation. Finally, the reaction of the equipment to the motion of the carrier, Γ_c, is the term responsible for the coupling. Because it is assumed that the primary structure has infinite impedance in comparison with the carrier, the reaction forces of the equipment do not excite the rigid-body modes. This way, the corresponding generalized forces are obtained by making the product with the flexural mode shapes only:

$$\Gamma_c = -\begin{bmatrix} 0 \\ \mathbf{\Phi}_f \end{bmatrix} \mathbf{F}_1 \tag{10}$$

Taking into account Eqs. (3–10), the coupled equations of the dynamics of the carrier and the load become

$$\begin{cases} \dot{\mathbf{a}} = \bar{\mathbf{Y}}_1 \left(\Gamma_0 + \Gamma_{\mathrm{ex}} - \begin{bmatrix} 0 \\ \mathbf{\Phi}_f \end{bmatrix} \mathbf{F}_1 \right) \\ \mathbf{F}_1 = \mathbf{Z}_e \mathbf{\Phi}^T \dot{\mathbf{a}} \end{cases} \tag{11}$$

Equations (11) can be solved for the force and acceleration at the interface. This requires the superposition of the modal responses and the use of the relation between velocity and acceleration in a harmonic motion. The result is

$$\begin{cases} \mathbf{F}_1 = \left(I + \mathbf{Z}_e \mathbf{\Phi}^T \bar{\mathbf{Y}}_1 \begin{bmatrix} 0 \\ \mathbf{\Phi}_f \end{bmatrix} \right)^{-1} \mathbf{Z}_e \mathbf{\Phi}^T \bar{\mathbf{Y}}_1 (\Gamma_0 + \Gamma_{\mathrm{ex}}) \\ \ddot{\mathbf{U}}_1 = j\omega \left(\mathbf{\Phi}^T \bar{\mathbf{Y}}_1 (\Gamma_0 + \Gamma_{\mathrm{ex}}) - \mathbf{\Phi}^T \bar{\mathbf{Y}}_1 \begin{bmatrix} 0 \\ \mathbf{\Phi}_f \end{bmatrix} \mathbf{F}_1 \right) \end{cases} \tag{12}$$

B. Modal Mobility of the Carrier

The modal mobility of the carrier is a diagonal matrix. The components referring to the rigid-body modes show a different behavior with frequency than the components referring to the flexural modes. For the rigid-body modes, the mobility must be defined consistently with the respective generalized forces. For the flexural modes, its definition results directly from the standard normal mode decomposition. Following this reasoning and assuming that energy is dissipated via a viscous mechanism, the diagonal components of the modal mobility matrix become

$$\bar{\mathbf{Y}}_1 = \begin{cases} \bar{\mathbf{Y}}_{r,n} = 1 \\ \bar{\mathbf{Y}}_{f,n} = \frac{j\omega}{\omega_n^2 - \omega^2 + 2j\xi_n\omega_n\omega} \end{cases} \tag{13}$$

A hysteretic mechanism of damping can be assumed instead if the term $2j\xi_n\omega_n\omega$ in Eq. (13) is replaced by $j\zeta_n\omega_n^2$.

C. Impedance of Equipment

Girard and Imbert [22] showed that for a hard-mounted structure, the reaction force to a base acceleration can be obtained by multiplying the apparent mass matrix by the vector containing the rigid-body base acceleration in the six degrees of freedom:

$$\mathbf{F}_r = \tilde{\mathbf{M}} \ddot{\mathbf{U}}_r \tag{14}$$

The impedance matrix for an instrument relating force and velocity in the six DOF can thus be based on the concept of apparent mass and takes into account the relation between velocity and acceleration in a harmonic motion:

$$\mathbf{Z}_{e,k} = j\omega \tilde{\mathbf{M}}_k \tag{15}$$

In the case of a normalization of the mode shapes giving unitary modal mass and considering viscous damping, the apparent mass is a function of the modal participation factors, the frequency, and the residual mass of the higher-order modes:

$$\tilde{\mathbf{M}} = \mathbf{m}_B + \sum_{n=1}^{N} \mathbf{L}_n^T \mathbf{L}_n \frac{\omega_n^2 + 2j\xi_n\omega_n\omega}{(\omega_n^2 - \omega^2) + 2j\xi_n\omega_n\omega} \tag{16}$$

Assuming that there is no cross-coupling between interface points, the impedance matrix of the complete equipment set results from the assembly of the impedance matrices of each equipment unit, with the modal properties referring to the respective interface point:

$$\mathbf{Z}_e = \begin{bmatrix} [j\omega\tilde{\mathbf{M}}_1] & 0 & 0 \\ 0 & \ddots & 0 \\ 0 & 0 & [j\omega\tilde{\mathbf{M}}_K] \end{bmatrix} \tag{17}$$

D. Static Residual

The second term in the inverted matrix of Eq. (12) has a dependence on the number of flexural modes of the carrier that are retained and can be simplified to

$$\mathbf{Z}_e \mathbf{\Phi}_f^T \bar{\mathbf{Y}}_f \mathbf{\Phi}_f \tag{18}$$

The effects of truncation of the modal base can be minorated if the residual of the static contribution of stiffness is added:

$$\begin{cases} \mathbf{F}_1 = [I + \mathbf{Z}_e(\mathbf{\Phi}_f^T \bar{\mathbf{Y}}_f \mathbf{\Phi}_f + j\omega\mathbf{G}_{\mathrm{res}})]^{-1} \mathbf{Z}_e \mathbf{\Phi}^T \bar{\mathbf{Y}}_1 (\Gamma_0 + \Gamma_{\mathrm{ex}}) \\ \ddot{\mathbf{U}}_1 = j\omega[\mathbf{\Phi}^T \bar{\mathbf{Y}}_1 (\Gamma_0 + \Gamma_{\mathrm{ex}}) - (\mathbf{\Phi}_f^T \bar{\mathbf{Y}}_f \mathbf{\Phi}_f + j\omega\mathbf{G}_{\mathrm{res}}) \mathbf{F}_1] \end{cases} \tag{19}$$

The residual can be expressed in terms of the static compliance matrix. It is the difference between the static compliance between the interface points and the static compliance retained in the modal base according to Girard and Roy [23]. Having assumed unitary mass matrix normalization, the residual is given by

$$\mathbf{G}_{\text{res}} = \mathbf{G}_{I/F,kk'} - \sum_{n=1}^{N} \frac{\phi_{nk}\phi_{k'n}}{\omega_n^2} \tag{20}$$

The static compliance matrix relates forces and displacements between all the interface points and can be obtained via a static analysis or a static test.

E. Generalized Forces

For the case of the base acceleration, Girard and Imbert [22,24] defined the generalized forces that act on the flexural modes in terms of the modal participation factors. On the other hand, it will be useful to define the generalized forces that act on the rigid-body modes consistently with the rigid-body mode shapes and the rigid-body mobility defined in Eq. (13). The generalized forces due to base excitation can thus be given by

$$\Gamma_0 = \begin{cases} \Gamma_{0,r} = \frac{1}{j\omega}\ddot{U}_0 \\ \Gamma_{0,f} = -L_{nr}\ddot{U}_0 \end{cases} \tag{21}$$

In the case of the externally applied loads, only the flexural modes are assumed to be excited. This stems from the assumption that the primary structure has infinite impedance in comparison with the carrier structure. The generalized forces associated to the flexural modes are obtained by projecting the spatial distribution of the external force on the carrier mode shapes. Here, we consider concentrated loads, and the resulting generalized forces are thus

$$\Gamma_{\text{ex}} = \begin{cases} \Gamma_{\text{ex},r} = 0 \\ \Gamma_{\text{ex},f} = F_{\text{ex}}\phi_n(y) \end{cases} \tag{22}$$

F. Frequency Response Functions and Random Response

So far, the dependence on frequency has been omitted to avoid overloading the notation. At this point, it is useful to rewrite Eq. (19), putting in evidence the terms that depend on frequency:

$$\begin{cases} \mathbf{F}_1(\omega) = \{I + \mathbf{Z}_e(\omega)[\mathbf{\Phi}_f^T\bar{\mathbf{Y}}_f(\omega)\mathbf{\Phi}_f + j\omega\mathbf{G}_{\text{res}}]\}^{-1} \cdot \mathbf{Z}_e(\omega)\mathbf{\Phi}^T\bar{\mathbf{Y}}_1(\omega)[\Gamma_0(\omega) + \Gamma_{\text{ex}}(\omega)] \\ \ddot{\mathbf{U}}_\mathbf{1}(\omega) = j\omega\{\mathbf{\Phi}^T\bar{\mathbf{Y}}_1(\omega)[\Gamma_0(\omega) + \Gamma_{\text{ex}}(\omega)] - [\mathbf{\Phi}_f^T\bar{\mathbf{Y}}_f(\omega)\mathbf{\Phi}_f + j\omega\mathbf{G}_{\text{res}}]\mathbf{F}_1(\omega)\} \end{cases} \tag{23}$$

On the other hand, the frequency response functions of the interface force and acceleration can be expressed in terms of the base acceleration and external force through the transfer functions:

$$\begin{cases} \mathbf{F}_1(\omega) = H_{F,\ddot{U}}(\omega)\ddot{U}_0(\omega) + H_{F,F}(\omega)F_{\text{ex}}(\omega) \\ \ddot{\mathbf{U}}_\mathbf{1}(\omega) = H_{\ddot{U},\ddot{U}}(\omega)\ddot{U}_0(\omega) + H_{\ddot{U},F}(\omega)F_{\text{ex}}(\omega) \end{cases} \tag{24}$$

where

$$H_{F,\ddot{U}}(\omega) = [I + \mathbf{Z}_e(\omega)(\mathbf{\Phi}_f^T\bar{\mathbf{Y}}_f(\omega)\mathbf{\Phi}_f + j\omega\mathbf{G}_{\text{res}})]^{-1} \cdot \mathbf{Z}_e(\omega)\mathbf{\Phi}^T\bar{\mathbf{Y}}_1(\omega)\begin{bmatrix} \frac{1}{j\omega} \\ -L_{nr} \end{bmatrix} \tag{25}$$

$$H_{F,F}(\omega) = [I + \mathbf{Z}_e(\omega)(\mathbf{\Phi}_f^T\bar{\mathbf{Y}}_f(\omega)\mathbf{\Phi}_f + j\omega\mathbf{G}_{\text{res}})]^{-1} \cdot \mathbf{Z}_e(\omega)\mathbf{\Phi}^T\bar{\mathbf{Y}}_1(\omega)\begin{bmatrix} 0 \\ \phi(y_{\text{ex}}) \end{bmatrix} \tag{26}$$

$$H_{\ddot{U},\ddot{U}}(\omega) = j\omega\left[\mathbf{\Phi}^T\bar{\mathbf{Y}}_1(\omega)\begin{bmatrix} \frac{1}{j\omega} \\ -L_{nr} \end{bmatrix} - (\mathbf{\Phi}_f^T\bar{\mathbf{Y}}_f(\omega)\mathbf{\Phi}_f + j\omega\mathbf{G}_{\text{res}})H_{F,\ddot{U}}(\omega)\right] \tag{27}$$

$$H_{\ddot{U},F}(\omega) = j\omega\left[\mathbf{\Phi}^T\bar{\mathbf{Y}}_1(\omega)\begin{bmatrix} 0 \\ \phi(y_{\text{ex}}) \end{bmatrix} - (\mathbf{\Phi}_f^T\bar{\mathbf{Y}}_f(\omega)\mathbf{\Phi}_f + j\omega\mathbf{G}_{\text{res}})H_{F,F}(\omega)\right] \tag{28}$$

Random signals are described in terms of their power spectral density. If the transfer functions are known, then the power spectral density of the response can be determined in terms of the power spectral density of the loading [19]. Assuming, for simplicity, that the sources of random vibration are uncorrelated, the response to the base excitation becomes

$$\begin{cases} S_{\mathbf{F}}(\omega) = H_{F,\ddot{U}}(\omega)H_{F,\ddot{U}}^*(\omega)S_{\ddot{U}0}(\omega) \\ S_{\ddot{\mathbf{U}}}(\omega) = H_{\ddot{U},\ddot{U}}(\omega)H_{\ddot{U},\ddot{U}}^*(\omega)S_{\ddot{U}0}(\omega) \end{cases} \tag{29}$$

And the response to the externally applied force becomes

$$\begin{cases} S_{\mathbf{F}}(\omega) = H_{F,F}(\omega)H_{F,F}^*(\omega)S_{F\text{ex}}(\omega) \\ S_{\ddot{\mathbf{U}}}(\omega) = H_{\ddot{U},F}(\omega)H_{\ddot{U},F}^*(\omega)S_{F\text{ex}}(\omega) \end{cases} \tag{30}$$

G. Comments on the Numerical Implementation

When performing an implementation of the method derived earlier, the first step should consist of a modal characterization of the subsystems, which provides the data necessary to the computation of the impedance of the equipment units and the mobility of the carrier structure. In an early phase of the design, this can be accomplished by employing data from past similar projects or making analytical derivations based on simple models. In a more advanced phase of the project, results from a finite element analysis or from a test can be employed. It is important to notice that when the modal properties of carrier and loads are known, the coupled behavior is given by the impedance/mobility formulation, taking into account their mutual coupling without the need of another eigenmode computation.

For the instrument units, the natural frequencies and the modal participation factors of each mode must be determined with rigid interface condition. The impedance matrix is then obtained by applying Eqs. (16) and (17). In some situations, the equipment might be considered coupled to the carrier only via a one-degree-of-freedom interface (e.g. coupling to a panel in the out-of-plane direction). In this case, the system can be represented by a set of oscillators in parallel, in which the masses correspond to the out-of-plane effective masses of the system [22–24]. If, additionally, no coupling is considered between different interface points, then the impedance matrix $\mathbf{Z}_e$ becomes diagonal.

For the carrier structure, the natural frequencies, the modal participation factors, and the mode shapes are required. It is easier to

compute the natural modes of the carrier assuming free–free conditions at the interface with the equipment, especially if an analytical approach is being followed and the carrier is being represented by models of plates or beams. It also confers more flexibility in the design because different configurations of equipment distribution are possible given such a modal base of the carrier. However, in these boundary conditions, the convergence of the peak values and the resonances of the response require that a large number of normal modes of the subsystem be retained. This fact even compromises the accuracy of the coupled response because the computation of the higher-order modes is subject to considerable errors. This phenomenon is also observed in FEA condensation techniques. It is overcome by including the residuals of the static compliance of the carrier [24]. The static compliance between interface points must be determined analytically, numerically, or experimentally. It can be obtained by means of Eq. (20).

Equations (25) and (26) require a matrix inversion. However, the size of this matrix is limited to the number of interface points times the number of degrees of freedom at each interface, and therefore it raises no concerns from the numerical point of view. In summary, an implementation of the method consists of the following:

1) Determine the modal parameters of the subsystems:ω_n and L_{nr} for the equipment units and ω_n L_{nr} and $\mathbf{\Phi}_f$ for the carrier structure.

2) Compute the static compliance between interface points $\mathbf{G}_{I/F,kk}$ and the residual $\mathbf{G}_{\text{res}}$ for the carrier structure.

3) Compute the transfer functions for each frequency of interest with Eqs. (25–28).

4) Determine the PSD of the applied external loads or base excitation.

5) Compute the PSD of the coupled response by means of Eqs. (29) and (30).

6) Compute the rms of the response. For the case of a single instrument, the computation of the rms can be performed analytically.

All these operations require a significantly lower computational load when compared with standard FEM techniques.

IV. Numerical Example

The method was applied to predict the response of a satellite panel with equipment subject to a base excitation. This benchmark case consisted of the external panel 1B of the payload module of the MetOp spacecraft (Fig. 6). The structural panel consists of a honeycomb core sandwich composite. The mass of the panel alone is 26.8 kg, including harnesses. The properties of the panel were determined by finite element analysis, the modal properties by a modal analysis, and the static flexibility by a static analysis. Table 1 shows the obtained modal base.

Table 1 Modal base of MetOp PLM panel 1B

Natural frequency, Hz	
116.6	694.8
158.8	752.4
222.5	797.0
317.5	824.1
347.8	835.7
405.4	878.1
433.4	897.9
501.6	961.1
532.6	972.6
627.7	998.5
690.1	

There are eight boxes mounted on panel 1B. In this case, the predominant motion of the carrier structure consists of the out-of-plane bending of the panel. Also, no antennas or boomlike structures exist on the panel, thus the rotational motion was not considered. In the face of this, only the out-of-plane component of the mode shapes of the panel was retained and the instruments were represented by a set of oscillators in parallel with the mass of each oscillator equal to the effective mass of the respective normal mode in the out-of-plane direction. The modal properties of the instruments were estimated based on similarity to other instruments and from test results. Table 2 shows the modal bases assumed for each instrument.

The assessment of the accuracy of the method was performed in two steps. First, the effect of the static residual was evaluated by applying the method for the case of only one instrument mounted on the panel. This analysis was carried out with and without the residual. Instrument MEPED was simulated by a single oscillator. Its natural frequency was assumed to be equal to the first mode of the panel, and its mass was assumed as a parameter varying from 0 to 1000 kg.

Second, the results of applying the method to the panel mounted with eight instruments were compared with the results of a finite element analysis using Nastran. In both cases, the load case applied consisted of a base acceleration in the out-of-plane direction of the panel.

Figure 7 represents the relative error in rms between using or not using the static residual when computing the response to a unitary white-noise random base excitation. It can be observed that the influence of the static residual increases with the coupling as it increases with the mass of the instrument, and its omission in the computations can completely compromise the quality of the results.

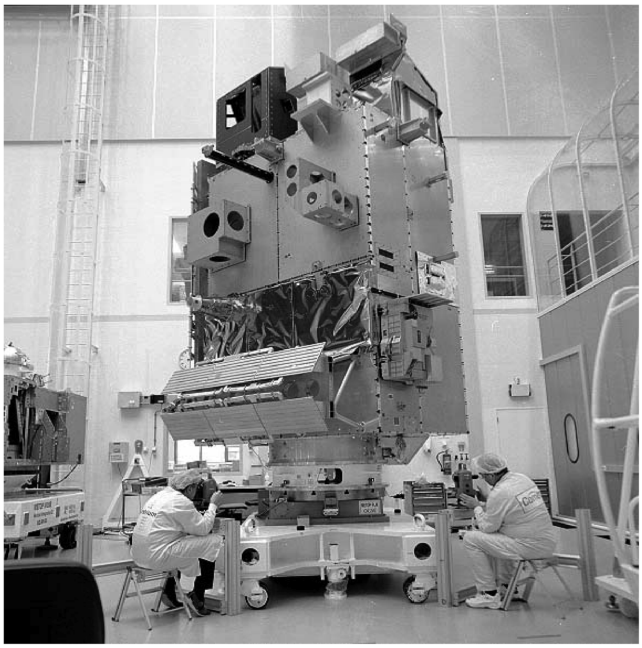

Fig. 6 MetOP payload module structural model (photo: ESA).

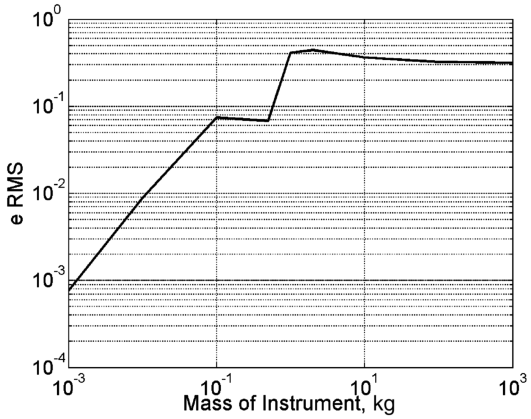

Fig. 7 Relative error in rms stemming from static contribution of the high-order modes.

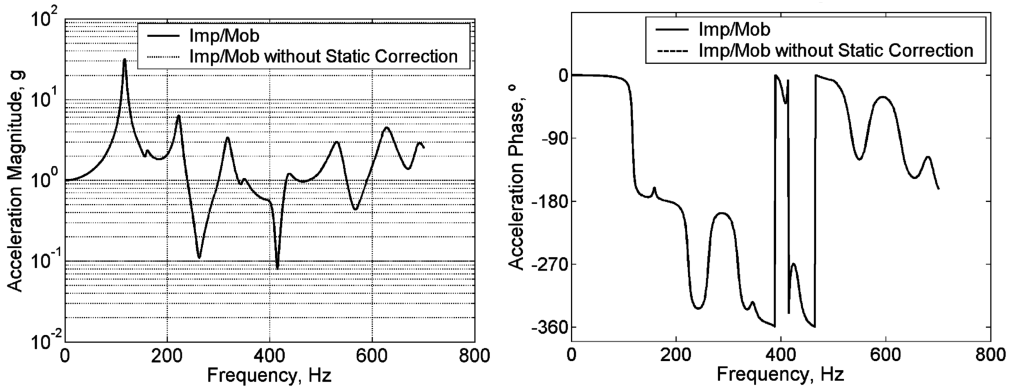

Fig. 8 Difference in FRF stemming from static contribution of the high-order modes. $m_{\text{inst}} = 0.0$ kg.

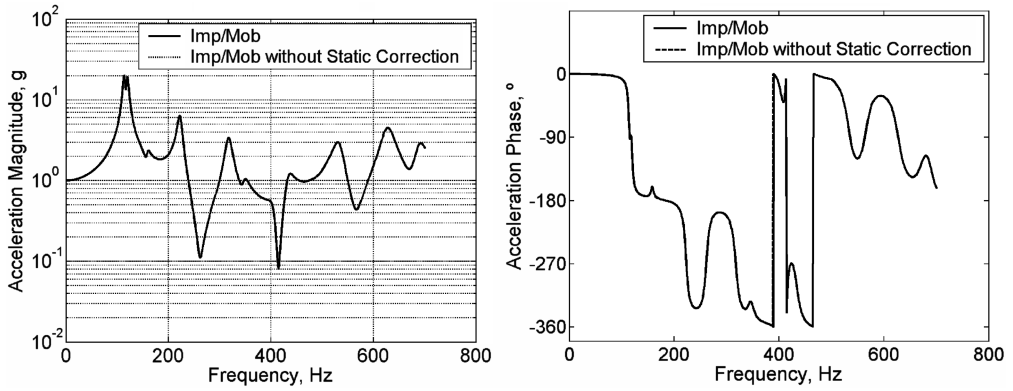

Fig. 9 Difference in FRF stemming from static contribution of the high-order modes. $m_{\text{inst}} = 0.0$ kg.

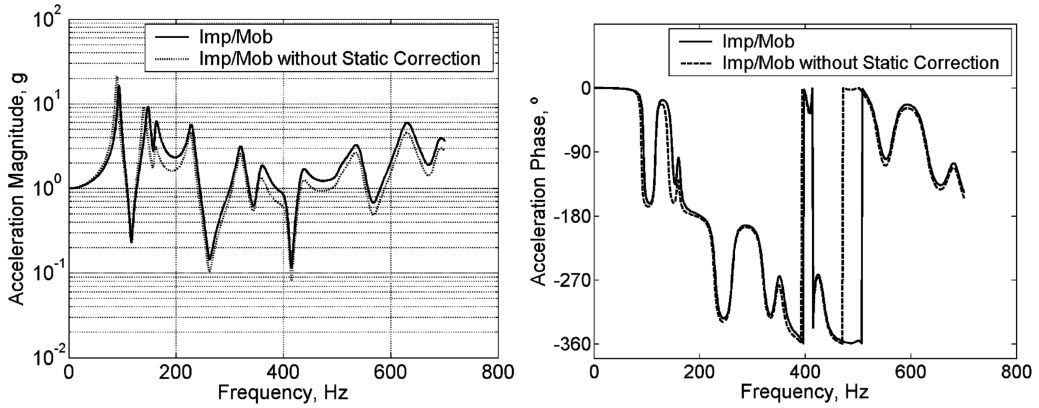

Fig. 10 Difference in FRF stemming from static contribution of the high-order modes. $m_{\text{inst}} = 0.0$ kg.

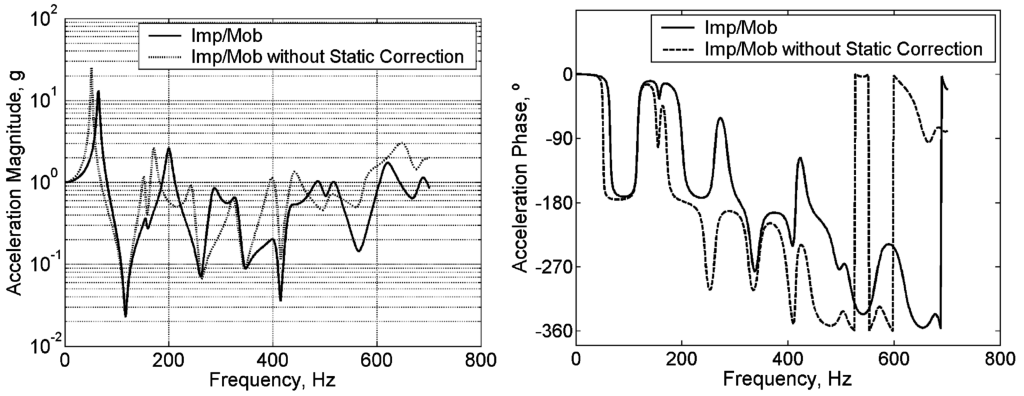

Fig. 11 Difference in FRF stemming from static contribution of the high-order modes. $m_{\text{inst}} = 0.0$ kg.

Table 2 Modal bases of the instruments mounted on MetOp PLM panel 1B

Instrument	Natural frequency, Hz	Effective mass, kg
MEPED	F1 = 253	.658
	F2 = 312	1.23
	F3 = 453	2.55
	F4 = 691	.658
	F5 = 820	1.89
	F6 = 940	1.23
EPC-A	F1 = 464	5.19
EPC-B	F1 = 464	5.19
DBU	F1 = 1249	.388
SSPA-A	F1 = 1099	3.19
SSPA-B	F1 = 1102	3.19
MPU	F1 = 305	7.98
HRS	F1 = 1250	.394

Moreover, Figs. 8–11 show that when the mass of the instrument increases, the response difference becomes larger and the contribution of the static residual becomes more important.

Finally, a comparison with the results obtained with MSC.Nastran was made for the case of the panel with eight boxes with the modal bases of Table 2 mounted on it. An excellent correlation with the solution provided by Nastran can be observed in Figs. 12–19. The differences observed between the two methods are due to the coupling of the modes of the panel above 1000 Hz and the modes of the instruments. This coupling is accurately captured by Nastran provided that the mesh refinement of the panel is adequate. However, in the results shown herein for the implementation of the impedance/mobility method, the modal base of the panel was truncated at 1000 Hz, as shown in Table 1.

Table 3 presents the mismatch in rms. It was observed that increasing the modal base of the carrier produced a better correlation with the Nastran results.

V. Conclusions

In this paper, we derived an analytical condensation technique based on impedance and mobility that reveals to be very compact and modular. It is highly suitable for determining the random-vibration environment of spacecraft equipment. After the initial characterization of each subsystem separately, the coupled response of carrier and instruments can be determined, requiring only the inversion and multiplication of small size matrices. Additionally, the study of different configurations for the distribution of the equipment over the carrier, sensitivity studies on the modal properties of carrier and equipment, and the integration of models of the subsystems from different subcontractors can all be performed with reduced effort: namely, avoiding the detailed and heavy finite element analysis of the complete system. Moreover, this method allows for the integration of data from any source, be it simple analytical hand calculations, tables, results from detailed finite element analysis, or experimental measurements. The only approximations are the modeling of the equipment units, neglecting the elasticity at the interface and the truncation of the modal bases of both equipment units and carrier.

This method overcomes the limitations of the simple two-degree-of-freedom models because it accurately accounts for the non-white-noise inputs, for the interaction of several modes of the carrier structure with several modes of the instrument, and for the particular location of the instrument on the carrier structure. It also presents advantages with relation to recently proposed methods with greater complexity. It is applicable to cases of any number of instruments with any number of normal modes mounted on carriers with any number of normal modes, and its modular feature eases the communication between the subcontractors responsible for each subsystem.

The results obtained with this analytical condensation method were compared against a detailed finite element analysis of a fully coupled system. Good correlation between the two methods could be observed.

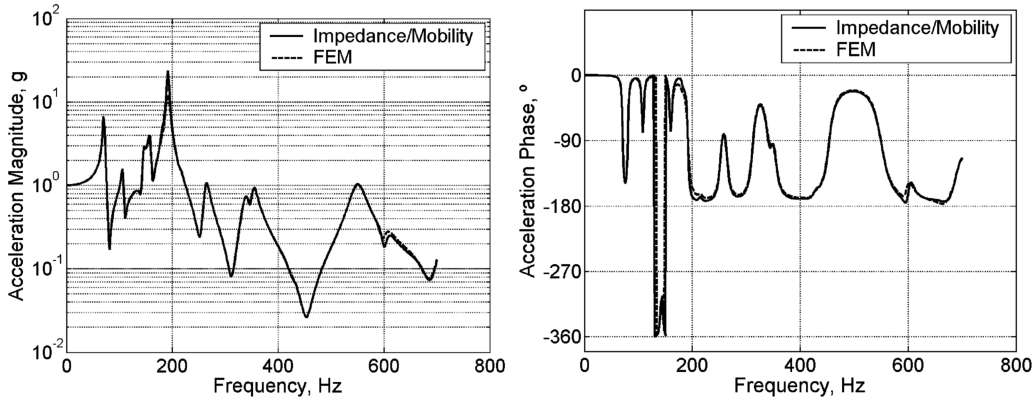

Fig. 12 Comparison of FRF with Nastran solution. Instrument MEPED.

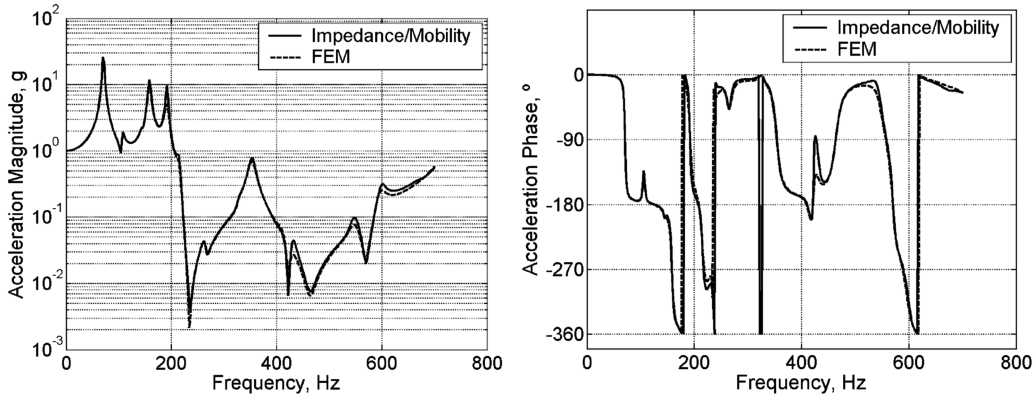

Fig. 13 Comparison of FRF with Nastran solution. Instrument EPC-A.

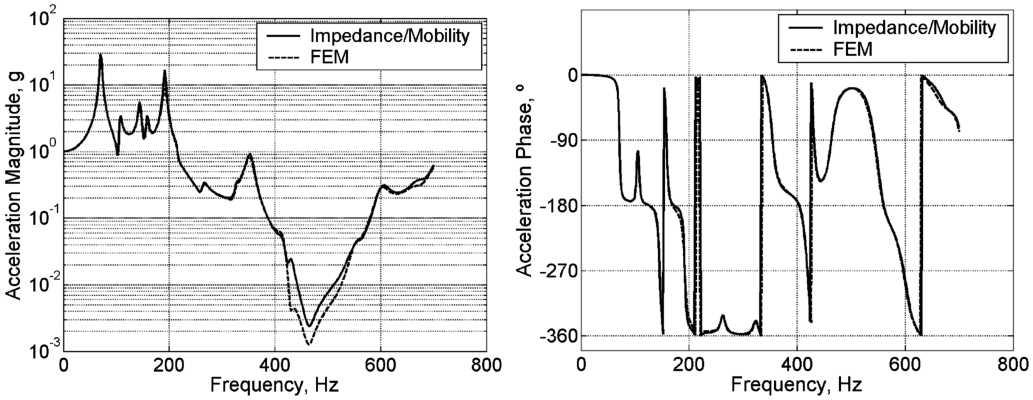

Fig. 14 Comparison of FRF with Nastran solution. Instrument EPC-B.

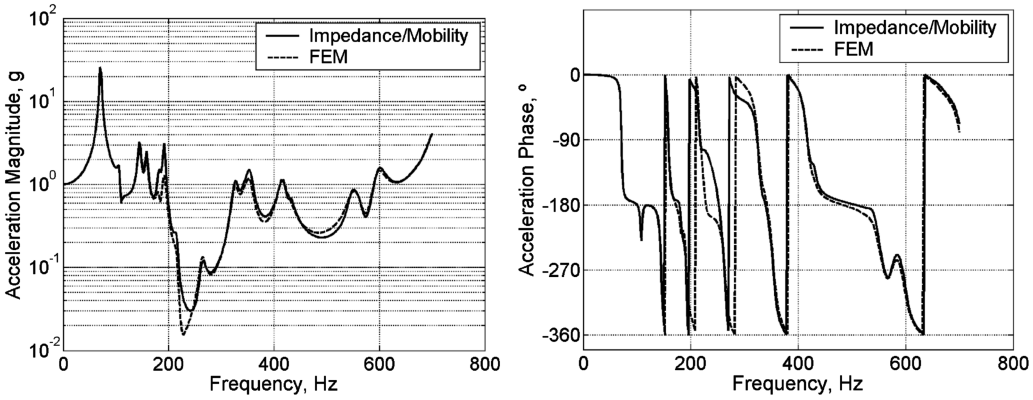

Fig. 15 Comparison of FRF with Nastran solution. Instrument DBU.

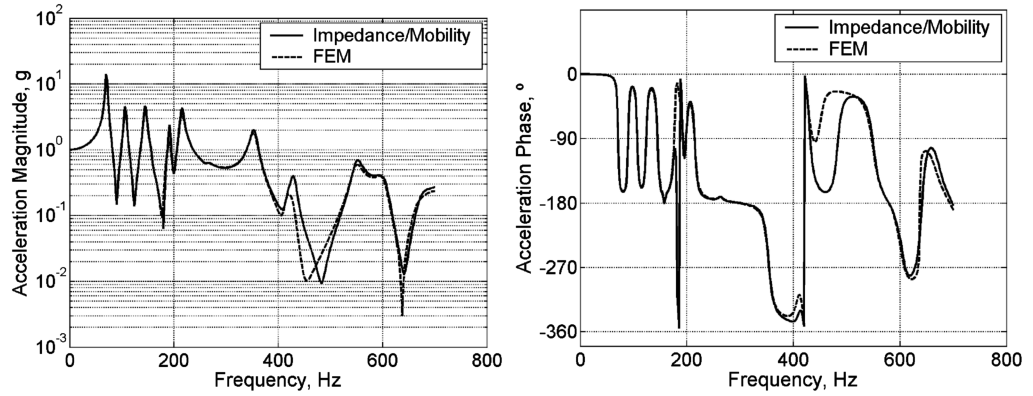

Fig. 16 Comparison of FRF with Nastran solution. Instrument SSPA-A.

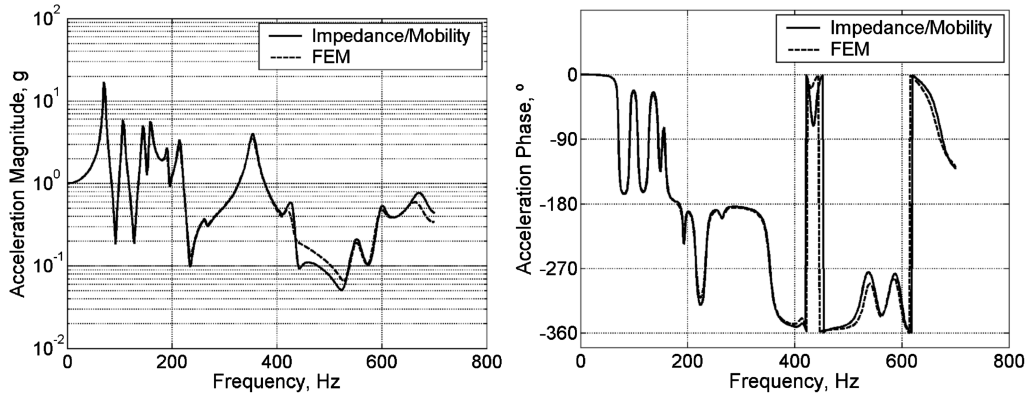

Fig. 17 Comparison of FRF with Nastran solution. Instrument SSPA-B.

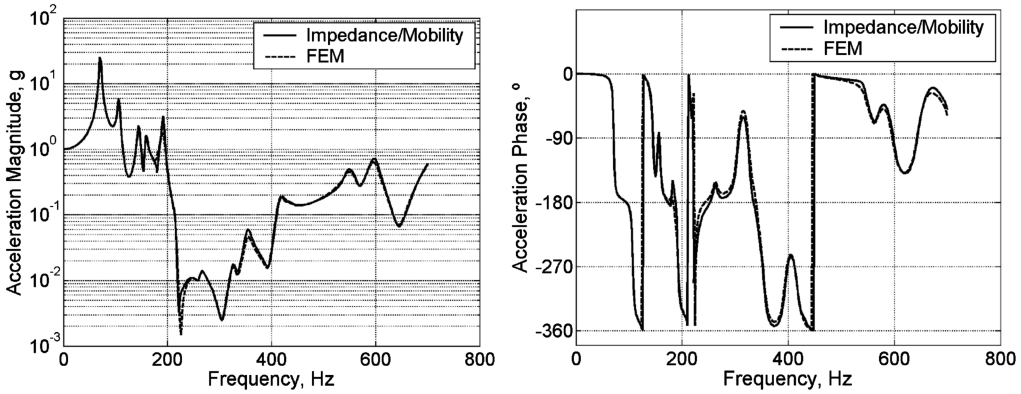

Fig. 18 Comparison of FRF with Nastran solution. Instrument MPU.

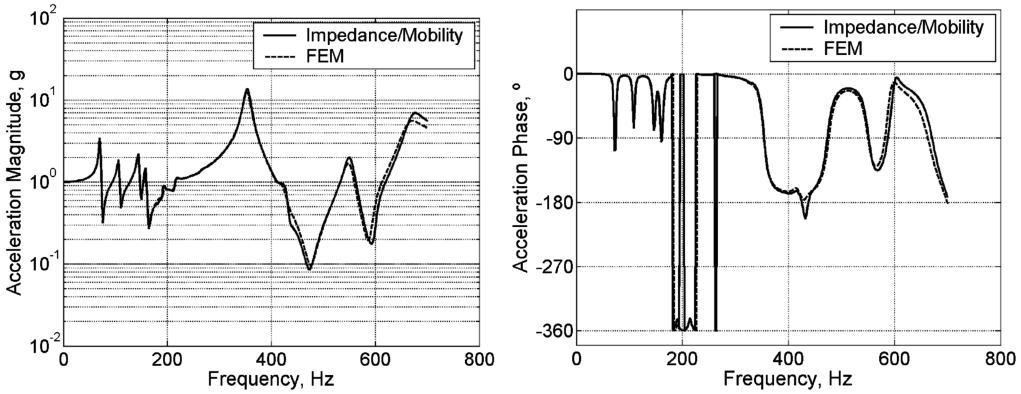

Fig. 19 Comparison of FRF with Nastran solution. Instrument HRS.

Table 3 Mismatch in rms[a]

RMS, g	Imp/Mob	Nastran
MEPED	66.06	45.18
EPC-A	73.90	69.02
EPC-B	83.58	75.39
DBU	65.87	64.42
SSPA-A	40.97	39.22
SSPA-B	52.48	50.24
MPU	62.82	61.55
HRS	79.22	71.07

[a]It was observed that increasing the modal base of the carrier produced a better correlation with the Nastran results.

Also, the importance of the static contribution of the high-order modes of the carrier on the accuracy of the coupled response was put in evidence. It was accounted for by computing the static residual of the compliance matrix of the carrier associated with the interface points to the instruments. A significant improvement was observed when comparing the situation without this residual (namely, with results presented by the authors in the past).

The next step of this condensation technique will consist of dealing with the more realistic case of distributed interfaces and the numerical implementation of cases with instruments with significant in-plane and rotational normal modes.

Acknowledgments

The authors wish to thank the Portuguese Foundation of Science and Technology for the traineeship program in the ESA European Space Research and Technology Center (ESTEC) (grant SFRH/BEST/7289/2002), S. Elliott and M. Brennan (Institute of Sound and Vibration Research) for fruitful discussions, and Graham Coe and Hans van de Graaf for the kind support.

References

[1] Troclet, B., Vanpeperstraete, S., and Schott, M.-O., "Experimental Analysis of Lift-Off and Aerodynamic Noise on the Ariane 5 Launch Vehicle," *DGLR-Bericht*, Vol. 1, No. 1, 1995, p. 535.

[2] Chemoul, B., Louaas, E., Roux, P., Schmitt, D., and Pourcher, M., "Ariane 5 Flight Environments," *Acta Astronautica*, Vol. 48, No. 5, 2001, pp. 275–285. doi:10.1016/S0094-5765(01)00026-1

[3] "Ariane 5 User's Manual," Arianespace, Evry–Courcouronnes, France, 2000.

[4] Miles, J. W., "On Structural Fatigue Under Random Loading," *Journal of the Aeronautical Sciences*, Vol. 21, No. 11, 1954, pp. 753–762.

[5] "Payload Flight Equipment Requirements and Guidelines for Safety Critical Structures," NASA SSP52005B, Dec. 1998.

[6] Van de Graaf, H., Santiago-Prowald, J., and Bureo, R., "The Application of Modal Effective Mass and Transmissibility Synthesis in Structural Analysis and Testing," *Proceedings of the European Conference on Spacecraft Structures, Materials and Mechanical Testing* [CD-ROM], ESA SP-581, ESA, Paris, 2005.

[7] Ceresetti, A., "Limit Load Factors Curve (LLF) for Preliminary Mechanical Design of Components for Space Missions—An Attempt of Mathematical Justification," *Proceedings of the European Conference on Spacecraft Structures, Materials and Mechanical Testing*, ESA SP-428, ESA, Paris, 1998, pp. 179–186.

[8] Chang, K. Y., "Force Limit Specifications vs. Design Limit Loads in Vibration Testing," *Proceedings of the European Conference on Spacecraft Structures, Materials and Mechanical Testing*, ESA SP-468, ESA, Paris, 2000, ESA, Paris, pp. 295–300.

[9] Scharton, T. D., "Force Limited Vibration Testing Monograph," NASA RP-1403, May 1997.

[10] Soucy, Y., and Côté, A., "Reduction of Overtesting During Vibration Tests of Space Hardware," *Canadian Aeronautics and Space Journal*, Vol. 48, No. 1, 2002, pp. 77–86.

[11] Ruotolo, R., and Cotterchio, M., "Evaluation of Flight Equipment Acceleration Caused by Random Vibration Loads," *AIAA Journal*, Vol. 39, No. 9, 2001, pp. 1758–1765.

[12] Ruotolo, R., "Extension of a Method for Determination of Flight Equipment Acceleration," *AIAA Journal*, Vol. 40, No. 7, 2002, pp. 1472–1474.

[13] Hixson, E., "Mechanical Impedance and Mobility," *Shock and Vibration Handbook*, edited by C. Harris, and C. Crede, McGraw–Hill, New York, 1987, Chap. 10.
[14] Gardonio, P., and Brennan, M. J., "On the Origins and Development of Mobility and Impedance Methods in Structural Dynamics," *Journal of Sound and Vibration*, Vol. 249, No. 3, 2002, pp. 557–573. doi:10.1006/jsvi.2001.3879
[15] Kim, S. M., and Brennan, M. J., "Modelling a Structural-Acoustic Coupled System with an Equivalent Lumped Parameter Mechanical System," *Journal of Vibration and Acoustics*, Vol. 121, Oct. 1999, pp. 453–459.
[16] Kim, S. M., and Brennan, M. J., "A Compact Matrix Formulation Using the Impedance and Mobility Approach for the Analysis of Structural-Acoustic Systems," *Journal of Sound and Vibration*, Vol. 223, No. 1, 1999, pp. 97–113. doi:10.1006/jsvi.1998.2096
[17] Rodrigues, G., and Santiago-Prowald, J., "Random Vibration Environment Derived from Acoustic Load Specifications," AIAA Paper 2004-2834, 2004.
[18] Brevart, B., and Pradines, A., "Comparison of Satellite Equipment Responses Induced by Acoustic and Random Vibration Tests," *Proceedings of the European Conference on Spacecraft Structures, Materials and Mechanical Testing* [CD-ROM], Centre National d'Etudes Spatiales, Toulouse, France, Dec. 2002.
[19] Newland, D., *An Introduction to Random Vibrations, Spectral And Wavelet Analysis*, 1st ed., Longman, Singapore, 1995, Chap. 7.
[20] Lou, M., "Structural Development of Flight Systems," *International Conference on Spacecraft Structures and Mechanical Testing*, ESA SP-321, ESA, Paris, 1991, pp. 559–566.
[21] Piersol, A., and Bendat, J., Engineering Applications of Correlation and Spectral Analysis, 2nd ed., Wiley, New York, 1980, Sec. 5.3.2.
[22] Girard, A., and Imbert, J., "Modal Effective Parameters and Truncation Effects in Structural Dynamics," *Proceedings of the 5th International Modal Analysis Conference*, Union College, New York, 1987, pp. 820–826.
[23] Girard, A., and Roy, N., "Modal Effective Parameters in Structural Dynamics," *Revue Européenne des Éléments Finis*, Vol. 6, No. 2, 1997, pp. 233–254.
[24] Girard, A., and Imbert, J., "Paramètres Modaux Effectifs et Effets de Troncature en Dynamique des Structures," *Proceedings of the Spacecraft Structures Conference*, ESA SP-238, ESA, Paris, 1985, pp. 81–86.

L. Peterson
Associate Editor